

Electronic-structure calculations of binary-alloy phase diagrams

Raymond J. Hawkins*

Henry Krumb School of Mines, Columbia University, New York, New York 10027

Mark O. Robbins†

Corporate Research Science Laboratories, Exxon Research and Engineering Company, Clinton Township, Route 22 East, Annandale, New Jersey 08801

J. M. Sanchez

Henry Krumb School of Mines, Columbia University, New York, New York 10027

(Received 13 August 1985)

A short-range-order—dependent electronic theory of coherent phase equilibrium in substitutional binary alloys is presented. The alloy internal energy is calculated using the cluster-Bethe-lattice method. The configurational entropy is evaluated using the cluster variation method. This approach is parameter free and uses only the results of elemental electronic-structure calculations as input. It is shown that the configuration dependence of the enthalpy of formation can be described by concentration-dependent effective pair interactions. Equilibrium phase diagrams for the Cr-W, Cr-Mo, and Mo-W systems are presented. Other thermodynamic properties can also be obtained. As an example, we calculate the chemical activities and high-temperature enthalpy of formation for the Cr-Mo system. The predicted phase diagrams and related thermodynamic functions are in good agreement with available experimental data.

I. INTRODUCTION

In an earlier paper¹ we presented a configuration-dependent microscopic theory of coherent phase equilibrium in substitutional binary alloys. Therein, an alloy free energy was constructed by coupling a tight-binding cluster-Bethe-lattice-method (CBLM) treatment²⁻⁴ of the electronic internal energy with Kikuchi's cluster-variation-method (CVM) treatment⁵ of the configurational entropy. In particular, it was shown that this CBLM-CVM approach predicted rather accurately the miscibility gap found in the Cr-W phase diagram.¹ In this paper we improve our previous CBLM-CVM treatment of the Cr-W system by describing the configurational entropy in the tetrahedron, rather than the pair, approximation of the CVM, and by allowing for asymmetry with respect to concentration in the analytic representation of the alloy internal energy. This improved theory is then applied to the Cr-Mo and Mo-W systems.

A common approach to the study of alloy phase equilibrium is to use phenomenological Ising- or pair-potential models for the internal energy together with a CVM treatment of the entropy. In some cases, these simple internal energy models together with the CVM give accurate results for alloy phase diagrams and related thermodynamic properties.⁵⁻¹² An important result of these studies has been the clear demonstration that atomic spatial correlations, particularly the Cowley short-range-order (SRO) parameter,¹³ play a crucial role in determining the equilibrium phase diagram.

More recently, first-principles treatments of the alloy internal energy have become available. However, in some

cases these were combined with the Gorsky-Bragg-Williams entropy approximation,¹⁴ which is known to introduce considerable error.¹⁵ For example, in bcc Ising systems the error in the transition temperature is about 20% for both phase separation and for L_2 ordering, and the approximation is qualitatively wrong for L_1 ordering in fcc lattices. This makes "agreement" of such calculations with experiment suspect and complicates the comparison between theory and experiment.

Our approach is to combine a microscopic, parameter-free treatment of the internal energy together with an accurate treatment of the configurational entropy. Vibrational entropy contributions are neglected which, in view of the overall agreement of our calculations with experiment, appears to be a reasonable approximation for the systems investigated. In particular, SRO is included in both the internal energy and the entropy calculations. Our CBLM treatment of the internal energy, although not *ab initio*, requires only the results of pure-element *ab initio* calculations as input. Previous work has shown that this approach correctly reproduces trends in enthalpies of formation of alloys.²⁻⁴ Furthermore, the CBLM together with the CVM has also been used to calculate some thermodynamic properties of the Cu-Au, Cu-Ag, and Ag-Au systems at fixed stoichiometries,¹⁶ to study the Co-Fe system¹⁷ and, more recently, has been found to predict accurately the Cr-W phase diagram.¹

Several other techniques for calculation of the electronic internal energy of alloys with SRO hold promise for future work. Some of these techniques, such as those of Connolly and Williams¹⁸ and the embedded-cluster Korringa-Kohn-Rostoker coherent-potential approxima-

tion (KKR CPA),¹⁹ are based on truly *ab initio* electronic-structure methods. However, these techniques rely heavily on the extrapolation of results from specific alloy configurations using effective cluster interactions such as those used in phenomenological theories. Stoichiometric ordered compounds have been used as reference states by Connolly and Williams.¹⁸ A more commonly used approach consists of extrapolation from a totally random state (calculated, for example, in the coherent-potential approximation). For example, in the generalized perturbation method (GPM) proposed by Gautier and co-workers,²⁰ cluster interactions are calculated from perturbations about the CPA medium. This technique has been investigated extensively in the tight-binding approximation and the results indicate that the alloy ordering energy is generally dominated by concentration-dependent effective pair interactions.²¹ In this context, one of the important results of the present work is that our values for the enthalpy of formation, which are calculated as an explicit function of SRO, can be described well by concentration-dependent effective pair interactions.

This paper is organized as follows: In Sec. II we present a brief review of the quantum- and statistical-mechanical approaches used in our calculations. We also discuss the representation of a portion of the alloy-mixing energy in terms of effective pair interactions and the evaluation of the phase diagram. In Sec. III we present the results of the calculations for the Cr-W, Cr-Mo, and Mo-W systems, and compare them with the available experimental data. Some concluding remarks are presented in Sec. IV.

II. THEORY

A. Hamiltonian

A tight-binding Hartree Hamiltonian was used which included both intersite and intrasite-Coulomb interactions.¹⁻⁴ This Hamiltonian incorporates the essential features required for a self-consistent treatment of charge transfer. It can be divided into three terms:

$$H = H_{1-e} - H_{e-e} + H_{\text{ion-ion}}, \quad (2.1)$$

where H_{1-e} is the one-electron tight-binding Hamiltonian, H_{e-e} is the electron-electron interaction (subtracted from the one-electron Hamiltonian since this interaction is counted twice in H_{1-e}), and $H_{\text{ion-ion}}$ is the interaction between the ions.

The one-electron tight-binding Hamiltonian incorporates the effective potential from the ions and other valence electrons due to charge transfer. We have employed a minimal tight-binding basis (one *s* orbital and five *d* orbitals; *s-d* hybridization included) of localized orthogonal orbitals centered on each atom. In terms of this basis,

$$H_{1-e} = \sum_{i,\beta} |i\beta\rangle E_{i\beta} \langle i\beta| + \sum_{i,\beta,j,\gamma} |i\beta\rangle t_{i\beta,j\gamma} \langle j\gamma|, \quad (2.2)$$

where $|i\beta\rangle$ is the ket for the orbital β at site i .

The diagonal Hamiltonian matrix elements $E_{i\beta}$ are as-

sumed to depend only on the species of atom I at the relevant site i . They are related to the intrinsic tight-binding onsite energies $E_{i\beta}^0$ by

$$E_{i\beta} = E_{i\beta}^0 + \bar{\Phi}_{i\beta}, \quad (2.3)$$

where $\bar{\Phi}_{i\beta}$ is the mean effective Coulomb potential seen by the β orbital on a type- I atom located at site i . This Coulomb potential is calculated in two parts: an intrasite contribution (effective direct-exchange energy) and an intersite contribution (effective Madelung energy) that is taken to be the same for all orbitals. The intersite contribution was evaluated using a direct summation method proposed by Robbins and Falicov.²⁻⁴

We have used atomic eigenvalues for the intrinsic onsite energies.²⁻⁴ These eigenvalues (listed in Table I) were calculated^{3,4} for a relativistic atom with one *s* electron and all *d* orbitals equally occupied. Exchange and correlation were included using the local-density functional calculated by Ceperley and Alder.²² Crystal-field splitting was not included. The eigenvalues do not include this spin polarization.

The off-diagonal Hamiltonian matrix elements or hopping energies, $t_{i\beta,j\gamma}$, are also assumed to depend only on the atomic species at the relevant sites, on the relative positions of the sites, and the character of the orbitals β and γ . Nearest- and next-nearest-neighbor hopping were included. The hopping energies between like species were evaluated from Harrison's Solid State Table²³ and are listed in Table I. Hopping energies between different species, $t_{A\beta,B\gamma}(\mathbf{r})$, were calculated using^{2-4,23}

$$t_{A\beta,B\gamma}(\mathbf{r}) = [t_{A\beta,A\beta}(\mathbf{r}) t_{B\gamma,B\gamma}(\mathbf{r})]^{1/2}. \quad (2.4)$$

The electron-electron and ion-ion interactions per atom are written

$$H_{e-e} = \frac{1}{2} \sum_I c_I \sum_{\beta,\gamma} u_I^{\beta\gamma} n_I^\beta n_I^\gamma + \frac{e^2}{N} \sum_{i,j} \sum_{\beta,\gamma} \frac{n_i^\beta n_j^\gamma}{2\epsilon r_{ij}}, \quad (2.5)$$

$$H_{\text{ion-ion}} = \frac{e^2}{N} \sum_{i,j} \frac{Z_i Z_j}{2\epsilon r_{ij}},$$

where c_I is the concentration of species I , $u_I^{\beta\gamma}$ are the effective direct-exchange interactions,^{2,4} n_I^β denotes the electron occupation of orbital β for species I , $-|e|n_I^\beta$ and $|e|Z_i$ are, respectively, the β -orbital valence and ionic charges at site i , ϵ is the dielectric constant, and r_{ij} is the distance between sites i and j . As shown by Robbins and Falicov,^{3,4} the difference $H_{\text{ion-ion}} - H_{e-e}$ largely cancels and can be written

$$H_{\text{ion-ion}} - H_{e-e} = -V\alpha(\sigma) \sum_I c_I (n_I - \frac{1}{2}\Delta n_I) \Delta n_I - \frac{1}{2} \sum_I c_I \sum_{\beta,\gamma} u_I^{\beta\gamma} n_I^\beta n_I^\gamma, \quad (2.6)$$

where V denotes the nearest-neighbor contribution to the average intersite potential per transferred electron, n_I is the total valence of species I , Δn_I is the total charge transfer to species I , and $\alpha(\sigma)$ is an effective Madelung sum which depends only on the Cowley SRO parameter σ . The SRO parameter σ is a measure of the degree of correlation between pairs of atoms. Values for σ range

TABLE I. Hamiltonian parameters in eV. We have used the notation of Slater and Koster (Ref. 51) for the overlap integrals. They are denoted by the type of orbital on each site, s and d , and the magnitude of the orbital's angular momentum m about the axis connecting the sites: σ , π , and δ correspond to $|m| = 0, 1, \text{ and } 2$, respectively. Integrals between n th-nearest neighbors have subscript n .

	Chromium	Molybdenum	Tungsten
Onsite			
E_s^0	-4.190	-4.320	-5.350
E_d^0	-3.140	-3.950	-3.560
Intersite			
$(ss\sigma)_1$	-1.707	-1.442	-1.421
$(sd\sigma)_1$	-0.833	-0.954	-1.013
$(dd\sigma)_1$	-0.921	-1.433	-1.637
$(dd\pi)_1$	+0.497	+0.774	+0.884
$(dd\delta)_1$	0.000	0.000	0.000
$(ss\sigma)_2$	-1.280	-1.082	-1.066
$(sd\sigma)_2$	-0.500	-0.572	-0.608
$(dd\sigma)_2$	-0.451	-0.702	-0.802
$(dd\pi)_2$	+0.244	+0.379	+0.443
$(dd\delta)_2$	0.000	0.000	0.000
Effective direct-exchange and Coulomb energies $u^{ss}=0.7, u^{sd}=0.9, u^{dd}=1.9, V=0.3$			

from $+1$, which corresponds to the completely segregated alloy, to -1 , which corresponds to a perfectly ordered stoichiometric CsCl structure. The values for V and $u_f^{\beta\gamma}$ used in our calculations are given in Table I. We have taken these parameters to be the same for all atomic species.²⁻⁴

B. Enthalpy of formation

The energy of central interest in our study is the enthalpy of formation, ΔH , defined by

$$\Delta H(\sigma, c) = H_{AB}(\sigma, c) - cH_A - (1-c)H_B, \quad (2.7)$$

where $H_{AB}(\sigma, c)$ denotes the total energy of alloy AB at concentration c of species A and SRO σ , and H_I denotes the energy of pure element I . The one-electron contribution to the total energy is related to the single-particle Green's function through the local density of states (LDOS). In terms of the LDOS, this contribution is written

$$\langle H_{1-e} \rangle = \int_{-\infty}^{\epsilon_F} [c\rho_A(\sigma, c, \omega) + (1-c)\rho_B(\sigma, c, \omega)]\omega d\omega, \quad (2.8)$$

where ϵ_F is the Fermi energy and $\rho_I(\sigma, c, \omega)$ is the LDOS for species I at energy ω , concentration c , and degree of SRO σ . The LDOS projected onto species I at site i is given by

$$\rho_I(\sigma, c, \omega) = -\frac{1}{\pi} \text{Im} \left[\sum_{\beta} \langle I\beta | \bar{G}(\sigma, c, \omega) | I\beta \rangle \right], \quad (2.9)$$

where the sum on β is taken over all orbitals, and where the overbar indicates configuration averaging of the single-site Green's function which, in turn, is defined by

$$G(\omega) = (\omega - H_{1-e})^{-1}. \quad (2.10)$$

In order to calculate the configuration-averaged Green's function at arbitrary concentration and arbitrary SRO, we have used the cluster-Bethe-lattice method.^{1-4, 16, 17, 24-26} The specifics of this approach are outlined in the Appendix. The alloy CBLM reproduces important features of the mean local chemical environment of all atoms in the alloy: the coordination number of the real lattice as well as the mean distribution of nearest neighbors. This mean-field approximation provides values for the total energy as a function of concentration and SRO. The SRO dependence is particularly important since it is from this that we shall obtain the effective pair interactions. Recently the CBLM has been shown to predict the zero-temperature stable-phase tendencies in transition- and simple-metal alloys.²⁻⁴ This approach also appears to predict correctly trends in the asymmetry of ΔH with respect to concentration.²⁷

After computation of the LDOS in the manner described in the Appendix, charge transfers [see Eqs. (2.5) and (2.6)] are determined and the resulting Coulomb interaction incorporated into the one-electron Hamiltonian using Eq. (2.3). The calculation of the LDOS is iterated until relative changes in the charge transfers are less than 10^{-4} , at which point electronic self-consistency has been

achieved. The electronically self-consistent total energy is then used to calculate $\Delta H(\sigma, c)$ at a given σ and c .

C. Configurational entropy

Equilibrium SRO is obtained by minimization of a properly constructed configurational free energy. To treat the configurational entropy of the alloy, we use the CVM, which provides a reasonably accurate description of

$$S = -k_B \left[6 \sum_{I,J,K,L} z_{IJKL} \ln(z_{IJKL}) - 12 \sum_{I,J,K} t_{IJK} \ln(t_{IJK}) + 3 \sum_{I,J} y_{IJ}^{(2)} \ln(y_{IJ}^{(2)}) + 4 \sum_{I,J} y_{IJ}^{(1)} \ln(y_{IJ}^{(1)}) - \sum_I x_I \ln(x_I) \right], \quad (2.11)$$

where k_B is Boltzmann's constant and z_{IJKL} , t_{IJK} , $y_{IJ}^{(k)}$, and x_I (collectively referred to as distribution variables) denote, respectively, the probability of finding tetrahedra, triangles, k th-neighbor pairs, and points in the configuration given by their subscripts (I equals A or B in a binary alloy). The distribution variables are related by the following consistency relations:

$$t_{IJK} = \sum_L z_{IJKL}, \quad (2.12a)$$

$$y_{IJ} = \sum_K t_{IJK}, \quad (2.12b)$$

$$x_I = \sum_J y_{IJ}. \quad (2.12c)$$

The Cowley SRO parameter¹³ (introduced above) for the k th neighbor, σ_k , is defined by the relation

$$\sigma_k = (x_A x_B - y_{AB}^{(k)}) / (x_A x_B). \quad (2.13)$$

The equilibrium value of the SRO parameter σ_k follows from the minimization, at constant concentration, of the configurational free energy

$$F = \Delta H - TS, \quad (2.14)$$

where ΔH and S are defined by Eqs. (2.7) and (2.11), respectively. Alternatively, we may minimize the grand

SRO.^{5-12,28-31} This nontrivial generalization of the mean-field approximation treats spatial atomic correlations (and, thus, SRO) within a chosen maximum cluster of lattice sites. The maximum cluster used in our study is the tetrahedron shown in Fig. 1 containing both first and second neighbors in the bcc lattice. In the tetrahedron approximation, the entropy for a bcc disordered system is written²⁹

potential Ω at constant chemical potential. The grand potential is defined by

$$\Omega = F - \mu \xi_1, \quad (2.15)$$

where μ is an effective chemical potential and ξ_1 is the point correlation function³⁰ given by

$$\xi_1 = x_A - x_B. \quad (2.16)$$

The minimization of the grand potential Ω is carried out as follows. We first calculate the alloy enthalpy of formation $\Delta H(\sigma, c)$ over a region of the σ - c plane in which we expect to find equilibrium. The calculated $\Delta H(\sigma, c)$ is then described (see Sec. IID) in this region by an analytic function of σ and c . This function is then used with Eqs. (2.11) and (2.15) to obtain an analytic closed-form expression for the grand potential which is finally minimized with respect to the distribution variables given in Eqs. (2.11) and (2.12a)–(2.12c) subject to the constraints

$$\sum_{I,J,K,L} z_{IJKL} = 1. \quad (2.17)$$

The resulting equilibrium values of σ_k and c are checked to ensure that they fall within the chosen σ - c region.

It may be shown that the equilibrium values, i.e., after minimization, of the effective chemical potential and grand potential can be written as

$$\mu = (\mu_A - \mu_B) / 2, \quad (2.18)$$

$$\Omega = (\mu_A + \mu_B) / 2, \quad (2.19)$$

where μ_I is the chemical potential of component I . Consequently, equilibrium between two phases, α and β , at a given temperature is determined by

$$\mu^\alpha = \mu^\beta, \quad (2.20)$$

$$\Omega^\alpha = \Omega^\beta. \quad (2.21)$$

D. Random energy and pair interactions

As discussed in the Introduction, effective pair interactions have been quite useful in phenomenological treatments of alloy phase equilibrium and arise naturally in other treatments of the electronic energy of alloys. To test this form and to facilitate the calculations we fit the

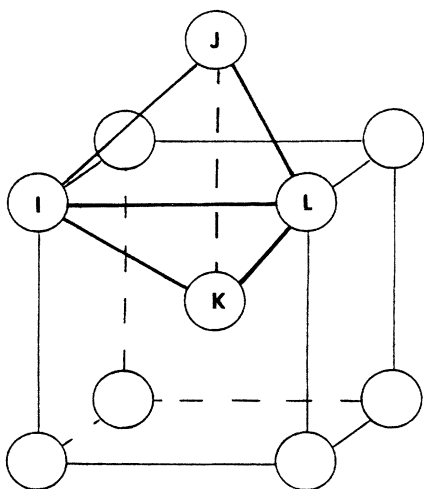


FIG. 1. Basic cluster for the bcc tetrahedron approximation.

CBLM results for $\Delta H(\sigma, c)$ with pair interactions. The enthalpy of formation $\Delta H(\sigma, c)$ is written as

$$\Delta H(\sigma, c) = E_{\text{rand}}(c) + E_{\text{ord}}(\sigma, c), \quad (2.22)$$

where $E_{\text{rand}}(c) = \Delta H(0, c)$ is the enthalpy of formation of the random alloy, and where the ordering energy E_{ord} takes into account the contributions due to short- and, if present, long-range order.

E_{rand} is a function only of the point correlation function ξ_1 .³⁰ In all alloys studied here, E_{rand} was found to be described well by the expression

$$E_{\text{rand}}(\xi_1) = (A_0 + B_0 \xi_1)(1 - \xi_1^2). \quad (2.23)$$

In terms of effective pair interactions, the ordering energy is written

$$E_{\text{ord}} = \frac{1}{2} \sum_k \omega_k V_k (\xi_2^{(k)} - \xi_1^2), \quad (2.24)$$

where ω_k , V_k , and $\xi_2^{(k)}$ are, respectively, the coordination number, effective pair interaction, and pair correlation function for the k th-nearest neighbor defined by

$$\xi_2^{(k)} = y_{AA}^{(k)} + y_{BB}^{(k)} - 2y_{AB}^{(k)}. \quad (2.25)$$

Noting that in terms of ξ_1 and $\xi_2^{(k)}$ the Cowley SRO parameter is written

$$\sigma_k = (\xi_2^{(k)} - \xi_1^2) / (1 - \xi_1^2), \quad (2.26)$$

Eq. (2.24) becomes

$$E_{\text{ord}}(\xi_1, \sigma_k) = \frac{1}{2} (1 - \xi_1^2) \sum_k \omega_k V_k \sigma_k, \quad (2.27)$$

where V_k is, in general, concentration dependent.

As shown below, in Cr-W, Cr-Mo, and Mo-W alloys, ΔH is found to be a rather linear function of SRO for fixed concentration. The first- and second-nearest-neighbor effective pair interactions are found to be fairly linear functions of concentration and they are approximated by the expression

$$V_k(\xi_1) = A_k + B_k \xi_1. \quad (2.28)$$

We find that the analytic expression for ΔH resulting from Eqs. (2.22)–(2.24) and (2.28) describes the calculated enthalpy of formation well over the region $0 \leq \sigma \leq 0.5$ and $0 \leq c \leq 1$, the root-mean-square deviations for the fits to ΔH being 4×10^{-2} , 5×10^{-2} , and 3×10^{-3} meV/atom, respectively, for Cr-W, Cr-Mo, and Mo-W. Parametrization of ΔH in this range of SRO was found to be sufficient for the systems investigated since, at all concentra-

tions and temperatures, the calculated equilibrium SRO was confined to the range $0 \leq \sigma \leq 0.2$. The parameters in Eqs. (2.23) and (2.28) were obtained by least-squares fitting of the calculated enthalpy of formation and they are given in Table II.

III. DISCUSSION AND RESULTS

A. Chromium-tungsten

The phase equilibrium of Cr-W was reviewed recently by Naidu, Sriramamurthy, and Rao.³² Cr-W is found experimentally to be a bcc-based isomorphous system. The experimental phase diagram reveals complete solid solubility between 1950 K and the solidus: below 1950 K a rather symmetric miscibility gap is found. Measurements of the alloy lattice parameter indicate that Cr-W has a slight positive deviation from Vegard's law.

The enthalpy of formation for Cr-W, calculated following the procedure described in Sec. II and using the parameters listed in Table I, is shown in Fig. 2 for different values of concentration and SRO. ΔH was found to be rather linear with respect to σ for fixed concentration, with a slight asymmetry with respect to concentration. This can be seen in Fig. 3, where the effective pair interactions for first- and second-nearest neighbors (V_1 and V_2 , respectively), determined using Eq. (2.24), are shown. V_1 is much larger (about 10 times) than V_2 and is a relatively weak linear function of concentration. Both V_1 and V_2 are negative, consistent with the fact that this alloy segregates at low temperature.

Owing to the lack of thermochemical measurements in this system,³² comparison between theory and experiment is limited to the phase boundary. The calculated phase diagram is compared to the experimental results^{32–36} in Fig. 4. The experimentally determined critical temperature is reproduced rather well in this calculation, the calculated critical temperature of 2140 K being 10% greater than the experimental critical temperature.

TABLE II. Enthalpy of formation parameters in eV.

	Cr-W	Cr-Mo	Mo-W
A_0	+ 0.106	+ 0.040	+ 0.005
B_0	– 0.005	+ 0.003	0.000
A_1	– 0.023	– 0.007	– 0.001
B_1	+ 0.003	– 0.001	0.000
A_2	– 0.002	0.001	0.000
B_2	– 0.002	+ 0.001	0.000

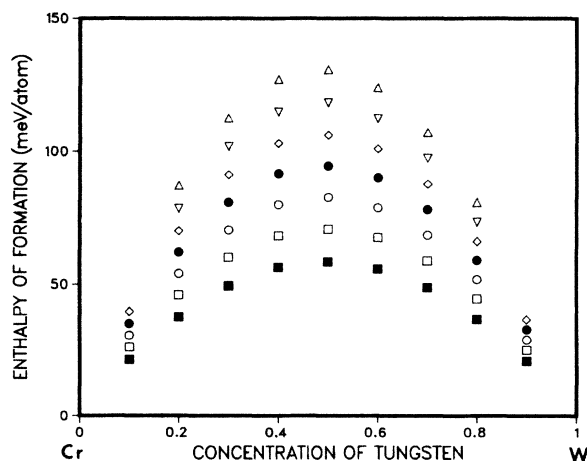


FIG. 2. Calculated enthalpy of formation at 0 K of Cr-W as a function of tungsten concentration for seven values of short-range order σ ($\sigma = -0.25$, \triangle ; $\sigma = -0.125$, ∇ ; $\sigma = 0$, \diamond ; $\sigma = +0.125$, \bullet ; $\sigma = +0.25$, \circ ; $\sigma = +0.375$, \square ; $\sigma = +0.5$, \blacksquare).

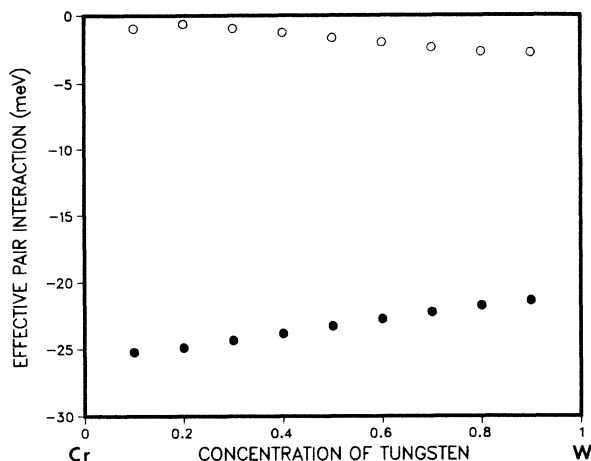


FIG. 3. First- (●) and second- (○) nearest-neighbor effective pair interactions of Cr-W as a function of tungsten concentration.

Although the experimental phase boundary appears quite symmetric, there is a positive deviation on the Cr-rich side. To explain this deviation within the context of the regular solution model an *ad hoc* strain energy was proposed in earlier work.³⁷ However, this proposal was countered by the equally tenable argument that the phenomenological regular solution description of the alloy internal energy was simply inadequate.³⁸ Our results are consistent with the latter view: In our treatment, the asymmetry in the Cr-W phase diagram arises naturally from the calculated electronic structure. The direction of the asymmetry is consistent with the trend found for alloys of monovalent simple metals which, like Cr, Mo, and W, are isoelectronic. Alloys with higher concentrations of the metal with the larger bandwidth are less strongly segregating (ΔH less positive). This trend is also found for Cr-Mo and Mo-W.

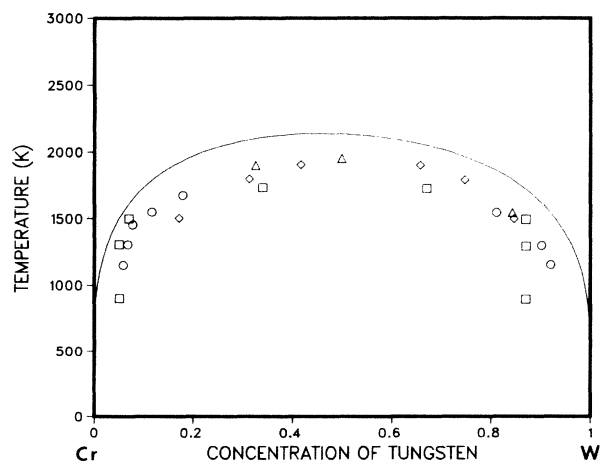


FIG. 4. Equilibrium phase diagram of Cr-W. The calculated phase boundary is shown by the solid curve. The experimental data indicated by the squares, circles, triangles, and diamonds are from Refs. 34, 35, 36, and 37, respectively.

To the authors' best knowledge, there are no experimental studies of the thermodynamic properties of Cr-W except for the phase diagram. Many other thermodynamic properties can be calculated with the CBLM and the CVM. Experimental data for the activities, enthalpy of formation, specific heat, and x-ray diffuse intensity would be quite useful in further assessing the predictive nature of the CBLM-CVM approach and of future first-principles treatments of alloy phase equilibrium.

B. Chromium-molybdenum

A review of the phase equilibrium of Cr-Mo has recently been completed by Venkatraman and Neumann.³⁹ Experimental studies of Cr-Mo (Refs. 40 and 41) indicate that this system is qualitatively similar to Cr-W: a bcc-based isomorphous system with a phase diagram characterized by a miscibility gap, and an alloy lattice parameter found to have a small positive deviation from Vegard's law. Unlike the Cr-W system, thermochemical measurements are available while direct measurements of the miscibility gap are limited. Measurements of the chemical activity and of the enthalpy of formation have been reported by Laffitte and Kubaschewski⁴² and Kubaschewski and Chart.⁴³ An x-ray study of phase separation in Cr-Mo at two concentrations has also been reported.⁴³

The enthalpy of formation for Cr-Mo, calculated following the procedure described in Sec. II using the parameters listed in Table I, is shown in Fig. 5 for different values of concentration and SRO. For Cr-Mo, the asymmetry with respect to concentration and the nonlinearity with respect to σ of ΔH are somewhat more pronounced than in the case of Cr-W. In Fig. 5 we see that ΔH peaks on the Cr-rich side. This asymmetry and the nonlinear dependence on σ are also evident in Fig. 6, where the effective pair interactions, calculated using Eq. (2.24), are shown. The relative variation in V_1 as a function of concentration is now about 30%, 3 times that of Cr-W, and the relative strength of V_2 to V_1 is double that seen in the

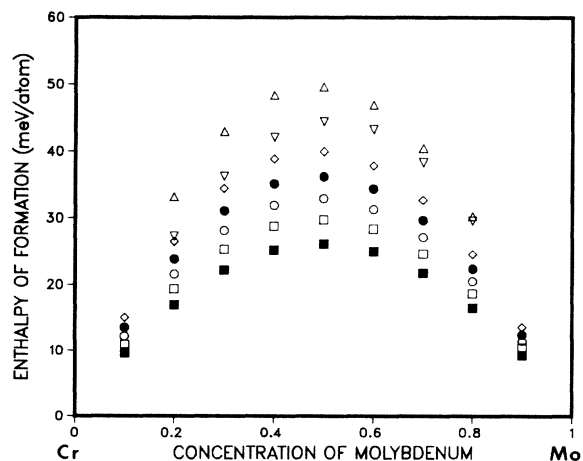


FIG. 5. Calculated enthalpy of formation at 0 K of Cr-Mo as a function of molybdenum concentration for seven values of short-range order ($\sigma = -0.25$, Δ ; $\sigma = -0.125$, ∇ ; $\sigma = 0$, \diamond ; $\sigma = +0.125$, \bullet ; $\sigma = +0.25$, \circ ; $\sigma = +0.375$, \square ; $\sigma = +0.5$, \blacksquare).

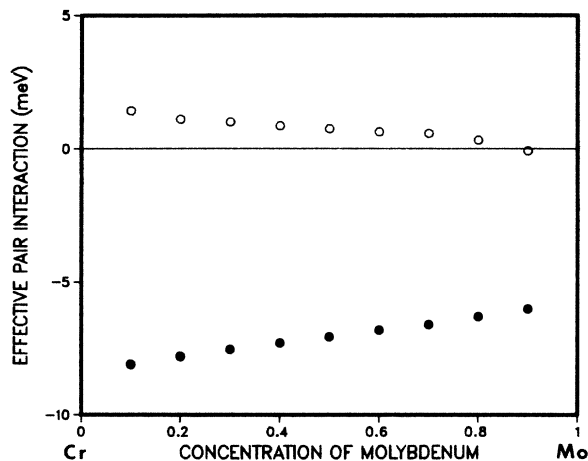


FIG. 6. First- (●) and second- (○) nearest-neighbor effective pair interactions of Cr-Mo as a function of molybdenum concentration.

Cr-W system. The sign of V_2 is also changed, but its magnitude is small enough that the internal energy remains consistent with a bcc segregating system.

The calculated chemical activities of Cr and Mo in the Cr-Mo alloy, given in terms of μ and Ω by

$$\begin{aligned} a_{\text{Cr}} &= e^{(\Omega + \mu)/k_B T}, \\ a_{\text{Mo}} &= e^{(\Omega - \mu)/k_B T}, \end{aligned} \quad (3.1)$$

are compared with experiment⁴² in Fig. 7. All of the qualitative features of the concentration dependence of these activities are predicted well by the theory. The close correspondence of experiment and theory is an indication that the alloy free energy is predicted correctly. The positive deviation from ideality of the activity reflects a positive excess free energy, indicative of a miscibility gap.

The calculated phase boundary in Cr-Mo is compared

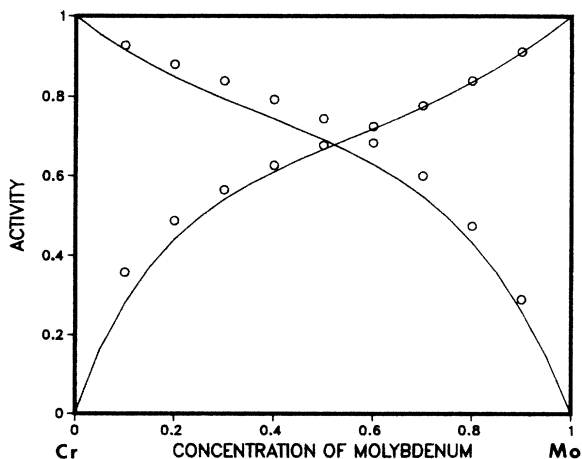


FIG. 7. Calculated activity of chromium and molybdenum in Cr-Mo as a function of molybdenum concentration. The open circles indicate the experimental data taken from Refs. 37 and 39.

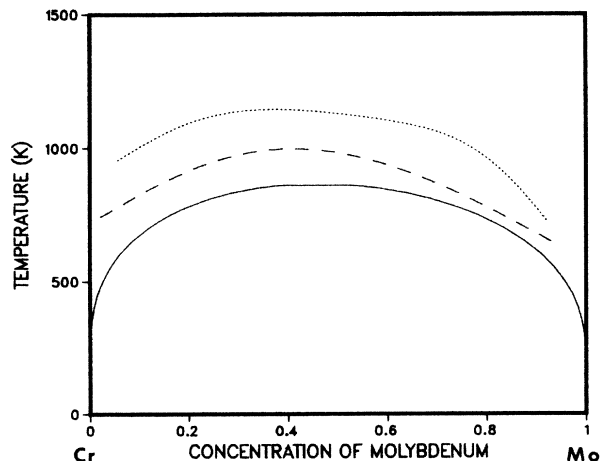


FIG. 8. Equilibrium phase diagram of Cr-Mo. The calculated phase boundary is shown by the solid curve. The assessed boundaries, the dashed and dotted lines, are from Refs. 39 and 37, respectively.

with two reported thermochemical assessments of the phase boundary in Fig. 8. The middle phase boundary was presented by Laffitte and Kubaschewski,⁴² who combined their measurements of the alloy free energy together with the Gorsky-Bragg-Williams approximation for the entropy. Our calculated critical temperature of 860 K differs from this assessment by 10%, well within the accuracy anticipated for the CBLM-CVM approach and their entropy approximation. The highest phase boundary was estimated by Kubaschewski and Chart.⁴³ These authors used the ΔH measurement shown in Fig. 9 with the alloy free energy measured by Laffitte and Kubaschewski⁴² to obtain the alloy entropy of mixing at 1400 K. To determine the miscibility gap, these authors assumed that both ΔH and the alloy entropy of mixing were temperature independent. The limited x-ray study mentioned previously is consistent with the resulting phase diagram. The top of the miscibility gap in their and other

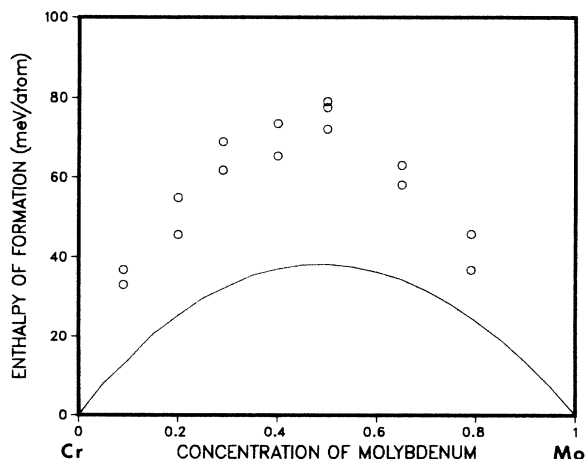


FIG. 9. Calculated equilibrium enthalpy of formation at 1400 K of Cr-Mo as a function of molybdenum concentration. The open circles indicate experimental data taken from Ref. 40.

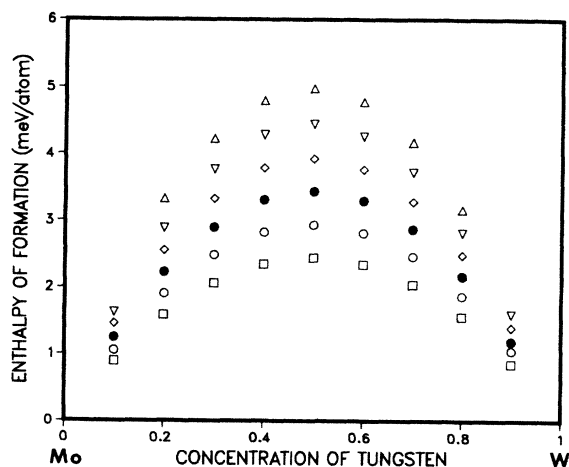


FIG. 10. Calculated enthalpy of formation at 0 K of Mo-W as a function of tungsten concentration for six values of short-range order σ ($\sigma = -0.125$, Δ ; $\sigma = 0$, ∇ ; $\sigma = +0.125$, \diamond ; $\sigma = +0.25$, \bullet ; $\sigma = +0.375$, \circ ; $\sigma = +0.5$, \square).

thermochemical calculations³⁹⁻⁴⁴ (all of which are based on these same two experiments) is located at 39 at. % Cr, which is consistent with our results. However, their thermochemical estimate of the critical temperature differs from our result by 27%.

Further experimental work would be helpful to clarify the apparently conflicting evidence concerning the location of the miscibility gap. It is surprising that while our calculated free energy (cf. Fig. 7) is in good agreement with experiment, the calculated values of the enthalpy of formation differ significantly from reported calorimetric measurements of this quantity (cf. Fig. 9). The two experimental measurements taken together imply a substantial nonconfigurational contribution to the entropy of mixing. Unfortunately a full description of the measurements of the enthalpy of formation has not been published and to

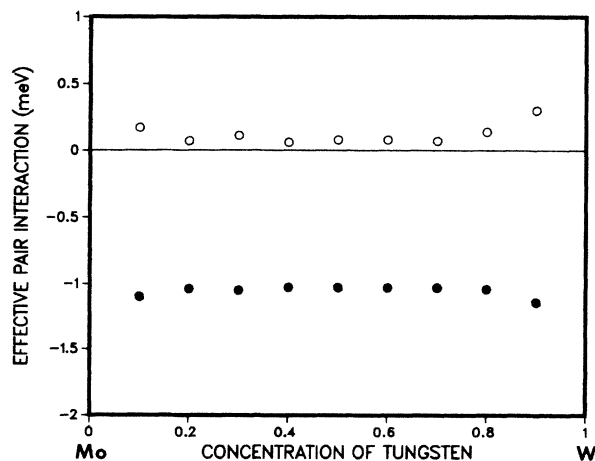


FIG. 11. First- (\bullet) and second- (\circ) nearest-neighbor effective pair interactions of Mo-W as a function of tungsten concentration.

the authors' best knowledge there are no experimental data for the entropy of mixing in Cr-Mo. Experimental studies of the thermodynamic properties of Cr-Mo at different temperatures would enable an assessment of this implied extra entropy term and would provide a clearer indication of the source of the apparent discrepancy between the calculated and experimental values for ΔH .

C. Molybdenum-tungsten

A recent review of the Mo-W system by Naidu, Sriramamurthy, and Rao⁴⁵ indicates that it, too, is a bcc-based isomorphous system. All cited x-ray studies have shown Mo-W to form a continuous series of solid solutions at all temperatures. Measurements of enthalpy⁴⁶ and of specific heat⁴⁷ in this system have all been found to obey an ideal law of mixing: any mixing contribution being below experimental resolution. There is some evidence, however, indicating the existence of a miscibility gap at low temperatures. In a study of diffuse x-ray scattering, Ol'shanskaya, Nekrasov, and Umanskii⁴⁸ reported positive values for the Cowley SRO parameter indicating clustering. Brewer⁴¹ has found that thermodynamic data for Mo-W indicate clustering with a miscibility gap below room temperature.

The enthalpy of formation for Mo-W, calculated following the procedure described in Sec. II using the parameters listed in Table I, is shown in Fig. 10 for different values of concentration and SRO. The effective pair interactions calculated using Eq. (2.24) are shown in Fig. 11. Although the effective pair interactions are of opposite sign, their ratio (V_2/V_1) is consistent with a bcc-based segregating system. Our calculation indicates that Mo-W segregates at low temperatures. The calculated values of ΔH (Fig. 10) indicate that the phase boundary should lie at temperatures about an order of magnitude lower than that of Cr-Mo. This is seen in Fig. 12, where we present the Mo-W phase diagram calculated using the effective pair interactions shown in Fig. 11. The low-temperature miscibility gap is consistent with the fact that experimental measurements of the enthalpy and specific heat at high

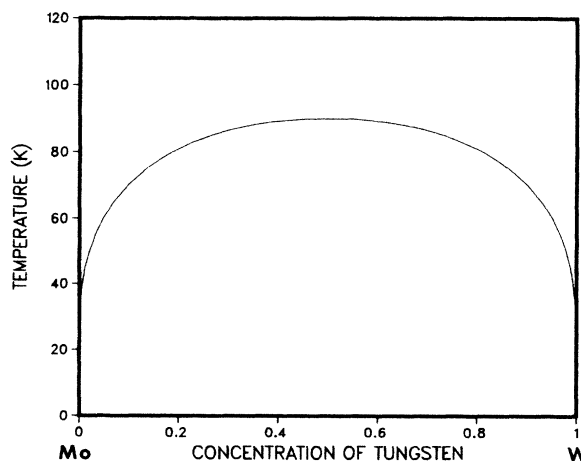


FIG. 12. Equilibrium phase diagram of Mo-W. The calculated phase boundary is shown by the solid curve.

temperature show no mixing contribution. Note that because Mo and W have similar bandwidths, ΔH and the phase diagram are very symmetric.

IV. CONCLUSIONS

We have calculated the equilibrium phase diagram and some related thermodynamic properties for the Cr-W, Cr-Mo, and Mo-W systems. In Cr-W the calculated phase diagram is in good agreement with experiment. A lack of experimental data precluded further comparative study in this system. In Cr-Mo, the calculated activities (and, consequently, the alloy free energy) are in good agreement with experiment. While the calculated and experimental high-temperature enthalpies of formation differ substantially, the predicted phase diagram is in reasonable agreement with thermochemical assessments. A low-temperature miscibility gap is predicted in Mo-W.

We found that the alloy enthalpy of formation was represented well by a function consisting of a nonlocal term describing the energy of the random alloy and an ordering term given by concentration-dependent effective pair interactions between first- and second-nearest neighbors. This description of ΔH is especially convenient for use with the CVM.

The trends in the phase diagrams can be understood in terms of previous studies of alloy enthalpies of formation. The main contributions to ΔH in transition-metal alloys come from the d bands. A mismatch in d -band widths provides a positive contribution to ΔH favoring segregation. The other main contribution to ΔH in transition-metal alloys is usually from hybridization of the two elemental d bands. However, this term is roughly proportional to ΔN_d^2 , where ΔN_d is the difference in the occupation of the elemental d bands. This term vanishes for the isoelectronic series Cr, Mo, W.⁴⁹ Thus, all three alloys segregate due to d -band mismatch. Other contributions to ΔH from charge transfer, s electrons, and s - d hybridization play a role in determining the magnitude of ΔH but are not dominant. The magnitude of ΔH increases from Mo-W to Cr-Mo to Cr-W as the size of the d -band width mismatch increases.

The miscibility gaps found in these systems are rather symmetric. This symmetry is peculiar to the alloys studied here and is not a general result. As observed by Watson *et al.*,⁵⁰ alloys of elements whose average d -band filling is near 50% tend to have symmetric phase diagrams, as do alloys of elements from the same column of the Periodic Table: Cr, Mo, and W satisfy both criteria. There is, nevertheless, a small asymmetry in the miscibility gaps which may be understood in terms of the mismatch between d -band widths. As shown for alloys of monovalent metals, alloys with more of the element with a larger bandwidth are less strongly segregating (ΔH less positive). This trend is seen in all three alloys studied. The asymmetry is very weak in Mo-W, where the d bandwidths are nearly equal, and increases in absolute magnitude as the mismatch increases in Cr-Mo and Cr-W.

In summary, we have presented a microscopic calculation of alloy phase equilibrium for binary transition-metal alloys that includes SRO explicitly. In this calculation we

begin with the electronic band structure of each alloy component and end with thermodynamic properties of the alloy that are in good agreement with experiment.

ACKNOWLEDGMENTS

The authors wish to thank M. Venkatraman and J. P. Neumann for providing a copy of their review of the Cr-Mo system prior to publication. Two of us (R.J.H. and J.M.S.) wish to acknowledge support by the National Science Foundation under Grants No. DMR-82-06195 and No. DMR-85-10594.

APPENDIX

The cluster-Bethe-lattice method is a real-space embedded-cluster technique. In the single-site approximation, the self-consistency condition is equivalent to solving the Hamiltonian on a Bethe lattice. For reasons discussed in Ref. 4, we treat the bcc lattice as having a coordination number of 14 with the eight nearest neighbors and the six second-nearest neighbors on the same shell. Using a single-atom cluster and a multiorbital basis, Dyson's equation

$$\omega \underline{G} = \underline{I} + \underline{H} \underline{G}, \quad (\text{A1})$$

where \underline{I} is the identity matrix, is solved by introducing a transfer matrix. This transfer matrix connects the Green's function on successive shells of atoms and is defined by

$$\underline{T}_{JK}(\mathbf{r}) = \underline{G}_{n,0}^{JI} (\underline{G}_{n-1,0}^{KI})^{-1}, \quad (\text{A2})$$

where \mathbf{r} denotes the vector connecting the sites of atoms K and J and n denotes the n th shell of atoms. In principle, this ratio of Green's functions depends on the occupation of other sites. In the CBLM a self-consistent mean-field approximation is made for these occupations which includes SRO through conditional pair probabilities defined by

$$P^{JL} = y_{JL} / x_J. \quad (\text{A3})$$

In this self-consistent mean-field approximation, Eqs. (A1) and (A2) yield

$$\underline{T}_{JK}(\mathbf{r}) = \left[\omega \underline{I} - \underline{E}_J - \sum_L P^{JL} \sum_{\mathbf{r}' \neq -\mathbf{r}} \underline{T}_{JL}(\mathbf{r}') \underline{T}_{LJ}(\mathbf{r}') \right]^{-1} \times \underline{T}_{JK}(-\mathbf{r}). \quad (\text{A4})$$

The equation for the site-diagonal element of the Green's function that determines the LDOS is

$$\underline{G}_{0,0}^J = \left[\omega \underline{I} - \underline{E}_J - \sum_L P^{JL} \sum_{\mathbf{r}} \underline{T}_{JL}(\mathbf{r}) \underline{T}_{LJ}(\mathbf{r}) \right]^{-1}. \quad (\text{A5})$$

The number of equations specified by Eq. (A4) can be halved by using the function^{3,4}

$$\underline{\beta}_J(\mathbf{r}) = \underline{T}_{JK}(\mathbf{r}) [\underline{T}_{JK}(-\mathbf{r})]^{-1} \quad (\text{A6})$$

which is independent of K . Further simplification of Eq. (A4) can be obtained using the symmetry of the hopping matrices.^{3,4} Equation (A4) is generally solved using fixed-point iteration which converges fastest at complex energies. Consequently, it is useful to convert the integral

in Eq. (2.8) into a contour integral in the complex plane. In addition to speed of convergence, the spectral function is a smoother function at complex energies, which results in more accurate as well as faster computation of integrals of the LDOS.

*Present address: Bell Communications Research, 331 Newman Springs Road, Red Bank, NJ 07701.

† Present address: Department of Physics and Astronomy, The Johns Hopkins University, Baltimore, MD 21218.

¹R. J. Hawkins, M. O. Robbins, and J. M. Sanchez, *Solid State Commun.* **55**, 253 (1985).

²M. O. Robbins and L. M. Falicov, *Phys. Rev. B* **25**, 2343 (1982).

³M. O. Robbins, Ph.D. thesis, University of California at Berkeley, 1983 (unpublished).

⁴M. O. Robbins and L. M. Falicov, *Phys. Rev. B* **29**, 1333 (1984).

⁵R. Kikuchi, *Phys. Rev.* **81**, 988 (1951); *J. Phys. (Paris) Colloq.* **38**, C7-307 (1977).

⁶C. Sigli and J. M. Sanchez, *CALPHAD* **8**, 221 (1984); *Acta Metall.* **33**, 1097 (1985); J. M. Sanchez, J. R. Barefoot, R. N. Jarrett, and J. K. Tien, *ibid.* **32**, 1519 (1984); J. M. Sanchez, R. N. Jarrett, C. Sigli, and J. K. Tien, in *High Temperature Alloys: Theory and Design*, edited by J. O. Stiegler (The Metallurgical Society of AIME, New York, 1984), pp. 83–101.

⁷J. M. Cowley, *Phys. Rev.* **77**, 669 (1950); *J. Appl. Phys.* **21**, 24 (1950).

⁸C. M. van Baal, *Physica (Utrecht)* **64**, 571 (1973).

⁹N. S. Golosov and A. M. Tolstik, *J. Phys. Chem. Solids* **37**, 279 (1976), and references therein; N. S. Golosov, A. M. Tolstik, and L. Ya. Pudan, *ibid.* **37**, 237 (1976), and references therein.

¹⁰J. M. Sanchez and D. de Fontaine, *Phys. Rev. B* **21**, 216 (1980); **25**, 1759 (1982); T. Mohri, J. M. Sanchez, and D. de Fontaine, *Acta Metall.* **33**, 1171 (1985).

¹¹R. Kikuchi and D. de Fontaine, in *Applications of Phase Diagrams in Metallurgy and Ceramics*, edited by G. C. Carter, NBS Publication No. SP-496 (U.S. GPO, Washington, D.C., 1978), p. 967; D. de Fontaine and R. Kikuchi, *ibid.*, p. 999.

¹²J. M. Sanchez and D. de Fontaine, *Phys. Rev. B* **21**, 216 (1980); **25**, 1759 (1982).

¹³R. Kikuchi, J. M. Sanchez, D. de Fontaine, and H. Yamauchi, *Acta Metall.* **28**, 651 (1980); A. deRoody, E. W. Van Royan, P. M. Bronsveld, and J. Th. M. de Hosson, *ibid.* **28**, 1339 (1980).

¹⁴J. Hafner, in *Alloy Phase Diagrams*, edited by L. H. Bennett, T. B. Massalski, and G. B. Giessen (North-Holland, New York, 1983), Vol. 19, pp. 1–15, and references therein.

¹⁵D. de Fontaine, in *Solid State Physics*, edited by H. Ehrenreich, F. Seitz, and D. Turnbull (Academic, New York, 1979), Vol. 34, and references therein.

¹⁶R. C. Kittler and L. M. Falicov, *Phys. Rev. B* **18**, 2506 (1978); **19**, 219 (1979); **19**, 527 (1979).

¹⁷F. L. Castillo-Alvarado, Ph.D. thesis, Instituto Politécnico Nacional, Mexico, 1984 (unpublished).

¹⁸J. W. D. Connolly and A. R. Williams, *Phys. Rev. B* **27**, 5169 (1983).

¹⁹A. Gonis, W. H. Butler, and G. M. Stocks, *Phys. Rev. Lett.* **50**, 1482 (1980); *Phys. Rev. B* **29**, 555 (1984).

²⁰F. Brouers, J. Giner, and J. Van der Rest, *J. Phys. F* **4**, 214 (1974); F. Gautier, F. Ducastelle, and J. Giner, *Philos. Mag.*

31, 1373 (1975); J. Giner, F. Brouers, F. Gautier, and J. Van der Rest, *J. Phys. F* **6**, 1281 (1976); F. Ducastelle and F. Gautier, *ibid.* **8**, 1437 (1978); A. Bieber and F. Gautier, in *Phase Transitions in Solids*, edited by T. Tsakalacos (North-Holland, New York, 1983), Vol. 21, pp. 331–336.

²¹A. Bieber, F. Gautier, G. Treglia, and F. Ducastelle, *Solid State Commun.* **39**, 149 (1981), and references therein.

²²D. M. Ceperley and B. J. Alder, *Phys. Rev. Lett.* **45**, 566 (1980).

²³W. A. Harrison, *Electronic Structure and the Properties of Solids* (Freeman, San Francisco, 1980).

²⁴J. D. Joannopoulos and F. Yñidurain, *Phys. Rev. B* **10**, 5164 (1974); L. M. Falicov and F. Yñidurain, *ibid.* **12**, 5664 (1975); F. Yñidurain and L. M. Falicov, *Solid State Commun.* **17**, 1545 (1975); P. N. Sen and F. Yñidurain, *Phys. Rev. B* **13**, 4387 (1976).

²⁵F. L. Castillo-Alvarado, J. L. Morán-López, and J. M. Sanchez, in *Phase Transformations in Solids*, edited by T. Tsakalacos (North-Holland, New York, 1983), Vol. 21, pp. 337–342.

²⁶M. F. Thorpe, in *Excitations in Disordered Systems*, edited by M. F. Thorpe (Plenum, New York, 1982), pp. 85–107.

²⁷M. O. Robbins (unpublished).

²⁸J. M. Sanchez, D. de Fontaine, and W. Teitler, *Phys. Rev. B* **26**, 1465 (1982).

²⁹R. Kikuchi, *J. Chem. Phys.* **66**, 3352 (1977).

³⁰J. M. Sanchez and D. de Fontaine, *Phys. Rev. B* **17**, 2926 (1978); J. M. Sanchez, F. Ducastelle, and D. Gratias, *Physica* **128A**, 334 (1984).

³¹R. Kikuchi, *J. Chem. Phys.* **60**, 1071 (1974); *Acta Metall.* **25**, 195 (1977).

³²S. V. Nagender Naidu, A. M. Sriramamurthy, and P. Rama Rao, *Bull. Alloy Phase Diagr.* **5**, 289 (1984).

³³W. Trzebiatowski, H. Ploszek, and J. Lobzowski, *Anal. Chem.* **19**, 93 (1947).

³⁴H. T. Greenaway, *J. Inst. Met.* **80**, 589 (1951–1952).

³⁵F. J. A. Den Broeder, *Acta Metall.* **20**, 319 (1972).

³⁶T. Margaria, C. Allibert, I. Ansara, and J. Driole, *High Temp.-High Pressures* **8**, 451 (1976).

³⁷A. D. McQuillan, *J. Inst. Met.* **80**, 694 (1951–1952).

³⁸H. T. Greenaway, *J. Inst. Met.* **80**, 694 (1951–1952).

³⁹M. Venkatraman and J. P. Neumann (unpublished).

⁴⁰R. Hultgren, P. D. Desai, D. T. Hawkins, and K. K. Kelly, *Selected Values of the Thermodynamic Properties of Binary Alloys* (American Society for Metals, Metals Park, Ohio, 1973), pp. 704–707.

⁴¹L. Brewer and R. H. Lamoreaux, in *Molybdenum: Physico-Chemical Properties of its Compounds and Alloys*, edited by L. Brewer (International Atomic Energy Agency, Vienna, 1980).

⁴²M. Laffitte and O. Kubaschewski, *Trans. Faraday Soc.* **57**, 932 (1961).

⁴³O. Kubaschewski and T. G. Chart, *J. Inst. Met.* **93**, 329 (1964–1965).

⁴⁴B. Gale and J. M. Davis, *Met. Sci.* **5**, 25 (1971).

⁴⁵S. V. Nagender Naidu, A. M. Sriramamurthy, and P. Rama Rao, *Bull. Alloy Phase Diagr.* **5**, 177 (1984).

- ⁴⁶V. Ya. Chekhovski, V. D. Tarasov, and I. A. Zhukova, *High Temp.-High Pressures* **2**, 59 (1970).
- ⁴⁷Yu. P. Zarichnyak, T. A. Lisnenko, and A. E. Basov, *Teplofiz, Vys. Temp.* **15**, 918 (1977).
- ⁴⁸E. Ya. Ol'shanskaya, Yu. V. Nekrasov, and Ya. S. Umanskii, *Akad. Nauk SSSR Bull. Phys. Ser.* **26**, 354 (1963).
- ⁴⁹D. G. Pettifor, *Phys. Rev. Lett.* **42**, 846 (1979); *Solid State Commun.* **28**, 621 (1978); in *Physics of Transition Metals*, edited by P. Rhodes (IOP, London, 1981), pp. 383–391.
- ⁵⁰R. E. Watson, L. H. Bennett, and D. A. Goodman, *Acta Metall.* **31**, 1285 (1983).
- ⁵¹J. C. Slater and G. F. Koster, *Phys. Rev.* **94**, 1498 (1954); corrected and extended to higher angular momenta by R. R. Sharma, *Phys. Rev. B* **19**, 2813 (1979).